Journal of Materials Chemistry A

Accepted Manuscript

This article can be cited before page numbers have been issued, to do this please use: H. Wang, S. Yin, Y. Xu, X. Li, A. A. Alshehri, Y. Yamauchi, H. Xue, Y. Kaneti and L. Wang, *J. Mater. Chem. A*, 2018, DOI: 10.1039/C8TA01698D.

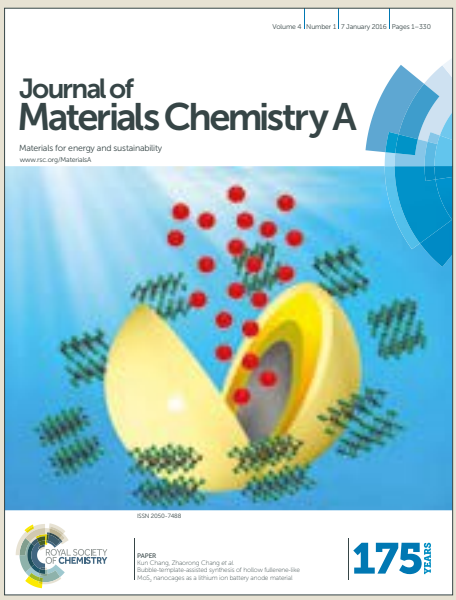

ROYAL SOCIETY OF CHEMISTRY

rsc.li/materials-a

View Article Online
DOI: 10.1039/C8TA01698D

Journal Name

ARTICLE

Direct fabrication of tri-metallic PtPdCu tripods with branched exteriors for oxygen reduction reaction

Received 00th January 20xx,
Accepted 00th January 20xx

DOI: 10.1039/x0xx00000x

www.rsc.org/

Hongjing Wang,[a] Shuli Yin,[a] You Xu,[a] Xiaonian Li,[a] Abdulmohsen Ali Alshehri,[b] Yusuke Yamauchi,[c,d] Hairong Xue,*[a] Yusuf Valentino Kaneti,*[e,f] and Liang Wang*[a]

Design of mutil-metallic nanocrystals with branched structures is very important for catalytic applications. Herein, a one-step synthesis of unique tri-metallic PtPdCu tripods with branched exteriors (PtPdCu TPs) in an aqueous solution is presented. Benefiting from its spatially and locally separated branches and tri-metallic compositions, the PtPdCu TPs exhibit superior activity and durability for oxygen reduction reaction. The newly designed PtPdCu TPs is quite different from previous tripods in its branched exteriors. The developed one-step method is very feasible for preparation of Pt-based mutil-metallic tripods with designed compositions and desired performances.

Introduction

Noble metal nanocrystals have attracted significant attention for energy conversion.[1-4] Among them, branched nanocrystals have received particular interest in various electrocatalytic applications, owing to their markedly improved activity and stability.[5-9] Tailoring of the size, morphology and composition provides an effective approach for obtaining branched nanocrystals with high electrocatalytic performance.[5,10-14] Specifically, the control of size and morphology offers favorable surface area and noble metal utilization, and the control of composition provides favorable electronic structure effect and synergistic enhancement effect.[1]

Among various branched noble metal-based nanocrystals, the tripods show obvious structural advantages for electrocatalysis.[15-18] The self-supported tripods are not susceptible to the Ostwald ripening/aggregation which results in the loss of active sites.[19-21] The open branches favor accessible surface and high permeability.[22-24] Many efforts have been devoted to the synthesis of metallic tripods, in which Pt-based tripods are highly desired.

To date, only very few methods have been developed to obtain Pt tripods, which mainly use galvanic replacement, seeded growth, and chemical etching.[25-30] These synthetic methods relies heavily on multi-step procedures, organic solvent, and high temperatures. As a result, they are difficult to be scaled up, and tend to generate low yield of Pt tripods. Therefore, the development of a facile and mild synthetic method for the synthesis of Pt tripods with a high yield is highly desired. It is expected that the decrease in size and the increase in length of the branches in Pt tripods can further improve the catalytic activity and Pt utilization. Moreover, it is noted that the surfaces of previously reported tripods were rather smooth.[25] The exquisite design of the tripod surface is highly important for further improving its active sites.

Pt-based tripods with controlled compositions have very rarely been demonstrated to date. The alloying of Pt with other metals can offer a favorable electronic effect which downshifts the Pt *d*-band center, resulting in the suppression of Pt oxides. The rational integration of Pt tripods with exquisitely designed surfaces and compositions will bring about a new Pt-based catalyst with high performance.

Inspired by this idea, herein, a one-step synthetic strategy is proposed for direct preparation of unique tri-metallic PtPdCu tripods with branched exteriors (PtPdCu TPs) in an aqueous solution with a high yield. The as-prepared PtPdCu TPs show high activity, superior durability and excellent methanol-tolerant ability for oxygen reduction reaction (ORR), attributed to their hierarchically branched structure and mutil-metallic compositions.

Experimental

Materials and chemicals. Sodium tetrachloropalladate (Na_2PdCl_4), L-ascorbic acid (AA), chloroplatinic acid hexahydrate ($H_2PtCl_6{\cdot}6H_2O$), Cupric chloride dihydrate

a *College of Chemical Engineering, Zhejiang University of Technology, Hangzhou, Zhejiang 310014, P.R. China.* *E-mail: xuehairong@zjut.edu.cn; wangliang@zjut.edu.cn
b *Department of Chemistry, King Abdulaziz University, P.O. Box. 80203, Jeddah 21589, Saudi Arabia.*
c *Department of Plant & Environmental New Resources, Kyung Hee University, 1732 Deogyeong-daero, Giheunggu, Yongin-si, Gyeonggi-do 446-701, South Korea.*
d *School of Chemical Engineering & Australian Institute for Bioengineering and Nanotechnology (AIBN), The University of Queensland, Brisbane, QLD 4072, Australia.*
e *College of Chemistry and Molecular Engineering, Qingdao University of Science and Technology, Qingdao 266042, China.*
f *International Center for Materials Nanoarchitectonics (WPI-MANA), National Institute for Materials Science (NIMS), 1-1 Namiki, Tsukuba, Ibaraki 305-0044, Japan.* E-mail: KANETI.Valentino@nims.go.jp

($CuCl_2 \cdot 2H_2O$), potassium bromide (KBr) and hydrochloride (HCl) were ordered from Aladdin (Shanghai, China). Pluronic F127 and commercial Pt/C (20 wt%) were purchased from Sigma-Aldrich and Alfa Aesar Co., respectively.

Synthesis of PtPdCu TPs. Typically, Na_2PdCl_4 (2.5 mL, 20 mM), $CuCl_2$ (1 mL, 20 mM), H_2PtCl_6 (1 mL, 20 mM), HCl (0.2 mL, 6 M), KBr (200 mg) and F127 (50 mg) were mixed and dissolved under sonication. After adding AA (2 mL, 0.1 M), the mixture solution was heated to 95 °C for 3 h. The PtPdCu TPs were obtained by centrifuging/washing with water for three times and then used for further characterizations.

Characterizations. The transmission electron microscope (TEM) (JEOL-2100F) equipped with energy-dispersive X-ray spectroscopy (EDS) was used to analyze the structure and composition of the samples. The Hitachi S-4800 scanning electron microscope (SEM) was used for investigation of the particle shape and size of the samples. X-ray diffraction (XRD) pattern was acquired by a D8 ADVANCE (Bruker AXS, Germany) with Cu-Kα radiation X-ray source (λ = 1.5406 Å). X-ray photoelectron spectra (XPS) measurements were carried out on ESCALAB MK II spectrometer (VG Scientific, UK) with Al-Kα X-ray excitation.

Electrochemical investigations. Electrochemical measurements were carried out by a CHI 760D (Chenhua Co., Shanghai, China) electrochemical analyzer with a traditional three-electrode cell, including a working electrode (rotating glassy carbon disk electrode, RDE), a reference electrode (Ag/AgCl electrode) and a counter electrode (Pt wire electrode). Cyclic voltammograms (CVs) and linear sweep voltammograms (LSVs) were employed. The working electrode was coated with 5 μL of ink (2 mg mL^{-1}) of catalyst and then dried. After that, 5 μL of Nafion (0.5 %) was dropped on the catalyst film and dried. RDE and Rotating ring-disk electrode (RRDE) measurements for ORR were performed in an O_2-saturated 0.1 M $HClO_4$ electrolyte with a rotation speed of 1600 rpm at a sweeping rate of 5 mV s^{-1}.

Koutecky-Levich equation was used to calculate the electron transfer number (n) which can be expressed as

$$\frac{1}{j} = \frac{1}{j_k} + \frac{1}{j_d}$$

Herein, j, j_k, and j_d represent measured, kinetic, and diffusion limiting current densities (mA cm^{-2}), respectively.

The diffusion limiting current densities (j_d) was expressed as

$$j_d = 0.2nFD^{2/3}\gamma^{-1/6}\omega^{1/2}\,C_{O2}$$

Herein, F (96485 C mol^{-1}) stands for the Faraday's constant. D (1.910 × 5 $cm^2\ s^{-1}$) indicates the diffusion coefficient of O_2. γ (1.13 × 10^{-2} $cm^2\ s^{-1}$) represents the kinetic viscosity. ω (rpm) is the rotation speed. And C_{O2} (1.2 × 10^{-3}mol m^{-3}) stands for the bulk concentration of O_2 dissolved in 0.1 M $HClO_4$.

The electron transfer number, n was determined by RRDE measurements consisting of I_D (disk current) and I_R (ring current), as follows:

$$n = \frac{4I_D}{(I_D + I_R/N)}$$

The hydrogen peroxide yield (% H_2O_2) was derived as follows:

$$\%H_2O_2 = \frac{200I_R}{(I_D N + I_R)}$$

Herein, N is the RRDE collection efficiency of the Pt ring determined to be 0.4286.

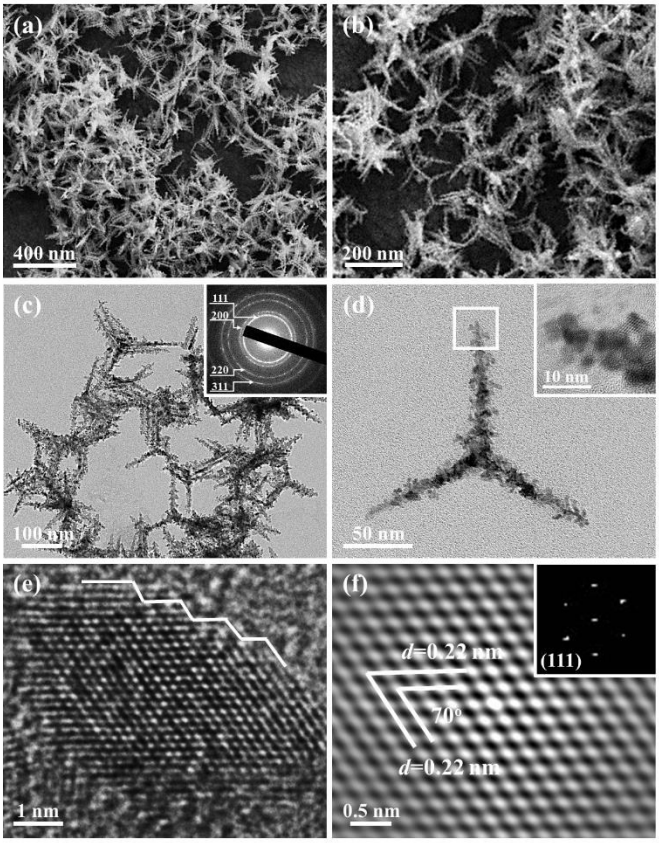

Fig. 1 (a and b) SEM images, (c and d) TEM images and (e) HRTEM image of the PtPdCu TPs. (f) Lattice fringe image. The inset in (c) shows SAED image, the inset in (d) shows HRTEM image of a branch, and the inset in (f) displays the corresponding FFT pattern.

Results and discussion

The PtPdCu TPs are directly obtained by a very simple thermal treatment of the reaction mixture aqueous solution. The yield of PtPdCu TPs is nearly 100 % (Fig. 1a-b). Each particle is assembled by spatially and locally separated three branches and the angle of adjacent branches is about 120°, which is a typical tripod structure (Fig. 1c-d). The PtPdCu TPs show a ring selected-area electron diffraction (SAED) pattern, indicating their polycrystalline nature (Inset in Fig. 1c). The width and length of each branch in PtPdCu TPs are around 13-18 nm and 75-88 nm, respectively. Interestingly, the exteriors of the tripod show a clearly branched structure (Fig. 1d). This is a very unique hierarchical branched structure, which is very different from previous metallic tripods with smooth surfaces.[25] The branched exteriors consisting of many small arms with sizes of 3–6 nm are highly porous, which provide sufficiently large exposed surface area (Inset in Fig. 1d). The distinct atomic steps can be clearly observed at the edge of the exteriors (Fig. 1e). The atomic steps are generally known to be highly active sites for ORR (Fig. 1e). The lattice fringes with 0.22 nm

View Article Online
DOI: 10.1039/C8TA01698D

intervals are attributable to the (111) plane of the face-centered-cube (*fcc)* structural PtPdCu alloy, implying that the Pt lattice is successfully incorporated with Pd and Cu atoms (Fig. 1f).

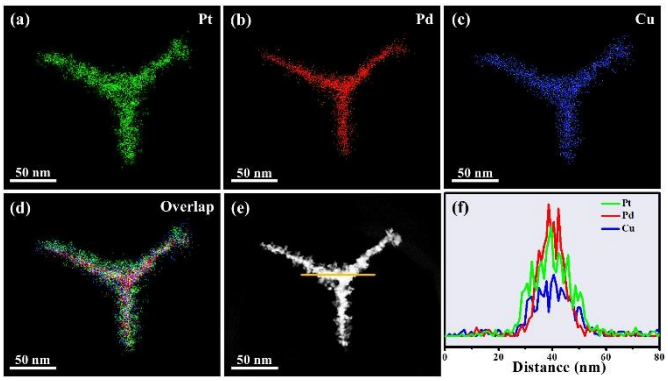

Fig. 2 (a-d) EDS mapping images and (e) HAADF-STEM image of a single PtPdCu TP. (f) The corresponding compositional line profiles.

Elemental mapping images and compositional line profiles of the PtPdCu TPs clearly reveal that Pt, Pd and Cu are well distributed throughout the hierarchical tripod shape, suggesting the alloy composition (Fig. 2). The atomic ratio of Pt/Pd/Cu is around 2/6/3 (Fig. S1a). The alloyed PtPdCu TPs is also confirmed by XRD investigation (Fig. 3a). The XRD pattern of the PtPdCu TPs exhibits five obvious diffraction peaks, which are assigned to metallic *fcc* structure. It is clear that no extra diffraction peaks for pure Pt, Pd, or Cu are detected, suggesting the well-alloyed single-phase PtPdCu nanocrystals without undesired phase separation. It is noted that these diffraction peaks slightly shift to higher angles relative to standard diffraction peaks of pure Pt or Pd, which resulted from the incorporation of the small sized Cu atoms into the *fcc* structure. XPS measurements are further carried out to confirm the valance states and surface compositions of the PtPdCu TPs. In the XPS spectrum of Pt, the four peaks at 71.3, 72.4 eV and 74.7, 76.1 eV center on the Pt 4f region can be attributed to Pt (0) and Pt(II), respectively (Fig. 3b). Interestingly, the binding energies for Pt $4f_{7/2}$ (71.3 and 72.4 eV) and Pt $4f_{5/2}$ (74.7 and 76.1 eV) slightly shift to a higher value relative to the pure Pt, indicating the modified electronic structure and lattice expansion/compression of Pt caused by the formation of PtPdCu alloy.[31-33] In the XPS spectrum of Pd, the two strong peaks for Pd $3d_{5/2}$ (340.9 eV) and Pd $3d_{3/2}$ (335.6 eV) are deconvoluted into four peaks, which indicate the presence of Pd (0) and Pd (II) species (Fig. 3c).[34,35] The peaks of Cu $2p_{3/2}$ and Cu $2p_{1/2}$ are observed in the XPS spectrum of Cu 2p. These peaks reveal the existence of Cu (0) and Cu (II) (Fig. 3d).[36,37] The XPS results therefore fully confirm that the PtPdCu TPs have been successfully prepared.

In order to explain the key factors for the formation of the PtPdCu TPs, a set of control experiments is performed. Without Cu^{2+}, irregular mono-metallic Pd and bi-metallic PtPd nanoparticles are produced, suggesting the key role of Cu^{2+} in the formation of the PtPdCu TPs (Fig. S2a-b). Because of the low stacking fault energy of Cu, the introduction of Cu^{2+} possibly stimulate the formation of plate-like seeds in the initial nucleation stage, which favors the subsequent growth into branched nanocrystals.[34] Meanwhile, Br^- is also important for controlling the structure. Irregular PtPdCu nanoparticles are obtained in the absence of Br^- (Fig. S2c). The Br^- can preferentially adsorb on the (100) facet of *fcc* metals, resulting in the growth of the nanocrystals along the (100) faces to be selectively prevented, which favors the branched metallic growth.[9] Without HCl, only irregular nanoparticles can be obtained (Fig. S3a), due to the fast rate of reaction. In the presence of HCl, the reducing capability of ascorbic acid is decreased. The slow metallic precursor reduction with slow metallic atom addition promotes growth of branched particles.[38] In the absence of F127, highly branched particles with larger sizes are produced in an aggregated form (Fig. S3b). The F127 not only serves as a capping agent, but also plays as a structural inducer role for the branched growth of Pt-based nanocrystals.[39]

With the decrease or increase in the amount of Pt precursor, pine needle-like nanoparticles (PtPdCu PNs) and multi-branched nanoparticles (PtPdCu MBs) are obtained with different Pt/Pd/Cu ratios (Fig. S1, Fig. S4a and Fig. S4c). But, the changes in particle size, dispersity, uniformity are observed relative to the typical PtPdCu TPs. The optimized metallic precursor amounts in the typical synthesis are suitable for high-quality preparation of the PtPdCu TPs with a high yield. A possible formation process of the PtPdCu TPs is speculated. In the initial stage of the reduction process, Pd nuclei are preferentially generated.[40] Subsequently, the Pd nuclei trigger the simultaneous co-reduction of Pt and Cu precursors by an autocatalytic process, which results in the formation of PtPdCu TPs. Therefore, the Pd is slightly concentrated at the centre of each branches, as shown in Fig. 2f. During the atomic addition process, the selected factors of Br^-, Cu^{2+}, HCl, and F127 facilitate the formation of the PtPdCu TPs.

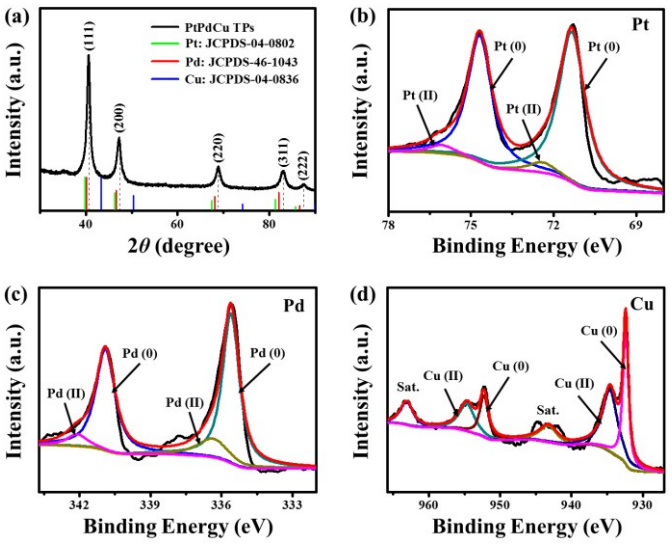

Fig . 3 (a) XRD pattern and (b, c, d) XPS spectra of the PtPdCu TPs.

Very few Pt tripods with smooth exteriors have previously been demonstrated, in which multi-step operation or harsh

DOI: 10.1039/C8TA01698D

reaction conditions are highly required. For instance, planar Pt tripods were synthesized via a two-step thermal treatment at 130 °C and 160 °C, respectively, in diphenyl ether solvent,[29] and tripod-like Pt nanostars were prepared at 150 °C in a pure oleylamine solvent with dihydrogen.[30] In comparison, the proposed one-step synthetic method in an aqueous solution is very simple for the high-quality preparation of tripods with a high yield. Moreover, the branched exteriors of the PtPdCu TPs are very different from previous Pt tripods with smooth surfaces, which are highly desired for a catalyst. Notably, the control of composition in metallic tripods has rarely been achieved. The proposed one-step method can easily fabricate tri-metallic PtPdCu tripods. The hierarchically self-supported structure of PtPdCu tripods is highly favorable for an electrocatalyst.

Inspired by the hierarchically branched structure combined with tri-metallic compositions, the PtPdCu TPs were investigated as an electrocatalyst for ORR, and benchmarked against PtPdCu PNs, PtPdCu MBs and commercial Pt/C catalyst in an acidic medium. The electrochemical active surface area (ECSA) of the PtPdCu TPs (39.29 $m^2\ g^{-1}$) is higher than those of PtPdCu MBs (36.3 $m^2\ g^{-1}$), PtPdCu PNs (15.19 $m^2\ g^{-1}$), and is close to Pt/C (43.8 $m^2\ g^{-1}$) (Fig. S5). For a comparsion, the ECSA of PtPdCu TPs (39.29 $m^2\ g^{-1}$) is also higher than previously reported PtPd nanoflowers (18.56 $m^2\ g^{-1}$),[41] Pt Nanoparticles (27 $m^2\ g^{-1}$),[42] PtCuCo ternary nanoalloys (22.99 $m^2\ g^{-1}$),[43] and PtCo nanomyriapods (24.49 $m^2\ g^{-1}$).[44] The hierarchically branched structure of the PtPdCu TPs provides high accessible surface, resulting in a higher ECSA. In the presence of O_2, there are obvious cathodic peaks in the CV curves for all of the samples, indicating a substantial ORR process (Fig. 4a). The onset potential (E_{onset}) and reduction peak potential (E_{peak}) of the PtPdCu TPs are the most positive during the ORR process relative to the compared samples (Fig. 4b). A higher limiting current density of the PtPdCu TPs (5.2 mA cm^{-2}) can be observed in comparsion with those of the PtPdCu MBs (4.7 mA cm^{-2}) and PtPdCu PNs (4.1 mA cm^{-2}), which is very similar to that of Pt/C (5.2 mA cm^{-2}). Moreover, the E_{onset} and half wave potential ($E_{1/2}$) (0.71, 0.65 V) of PtPdCu PTs are the most positive compared to those of PtPdCu MBs (0.69, 0.63 V), PtPdCu PNs (0.69, 0.64 V) and Pt/C (0.68, 0.61 V) (Fig. S6). The LSV results indicate the superior ORR catalytic activity of PtPdCu TPs. As a reference, the E_{onset} and $E_{1/2}$ of PtPdCu TPs (1.0 and 0.94 V *vs.* RHE) are more positive than those of previously reported Pt-based catalysts (Table S1). The specific activity of the PtPdCu TPs (1.03 mA cm^{-2}) is 2.0, 2.3 and 5.7 folds higher than those of the PtPdCu MBs (0.51 mA cm^{-2}), PtPdCu PNs (0.45 mA cm^{-2}), and Pt/C (0.18 mA cm^{-2}), respectively (Fig. S7).

The higher ORR activity of the PtPdCu PTs relative to the PtPdCu MBs and PtPdCu PNs are mainly ascribed to the following factors. Firstly, PtPdCu PTs show better particle dispersity and shape uniformity. Secondly, the PtPdCu PTs expose more surface area. Furthermore, the optimized ratio of Pt/Pd/Cu for the PtPdCu TPs favors an enhanced catalytic activity. The kinetics of the samples in ORR process is analyzed by Tafel plots. The obtained Tafel slopes for the PtPdCu TPs, PtPdCu MBs, PtPdCu PNs and Pt/C are 60, 77, 88, and 64 mV dec^{-1}, respectively. The PtPdCu TPs show the smallest Tafel slope, indicating that the transfer of the first electron is the rate determining step in the ORR process (Fig. 4c). For the sample with a low Tafel slope, it can be noted that the overpotential for ORR slowly rises with the increase in current density, implying that oxygen can be easily adsorbed and then activated on the catalyst surface.

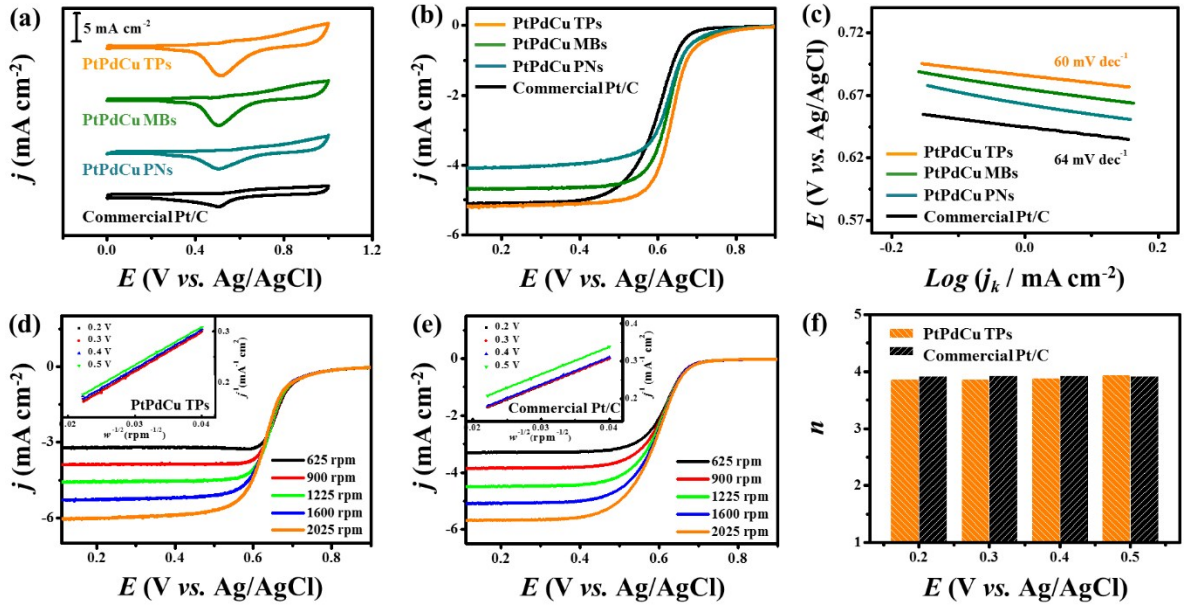

Fig. 4 (a) CV curves, (b) ORR polarization curves, and (c) Tafel slopes of the different catalysts. (d and e) ORR polarization curves with different RDE rotation rates, and the insets show the electron transfer numbers at different potentials. (f) The electron transfer numbers of the PtPdCu TPs and commercial Pt/C. All measurements were performed in an O_2-saturated 0.1 M $HClO_4$ electrolyte.

In order to further study the ORR kinetics, the LSV curves of the PtPdCu TPs and Pt/C were measured at various rotation rates (Fig. 4d and 4e). Their limiting current densities are rapidly increased with the increase in rotation rate. By using Koutecky-Levich equation, a good linear relation of the corresponding Koutecky-Levich plots for the the PtPdCu TPs can be found at the potentials of 0.2, 0.3, 0.4, and 0.5 V, indicating the first order of the ORR reaction kinetics on the PtPdCu TPs. The calculated *n* of the PtPdCu TPs are 3.86, 3.87, 3.89 and 3.94 at 0.2, 0.3, 0.4, and 0.5 V, respectively, which are similar to Pt/C (3.92, 3.93, 3.93 and 3.92) at the same potentials, indicating that the samples possess the one-step ORR kinetics through four-electron pathway (Fig. 4f).

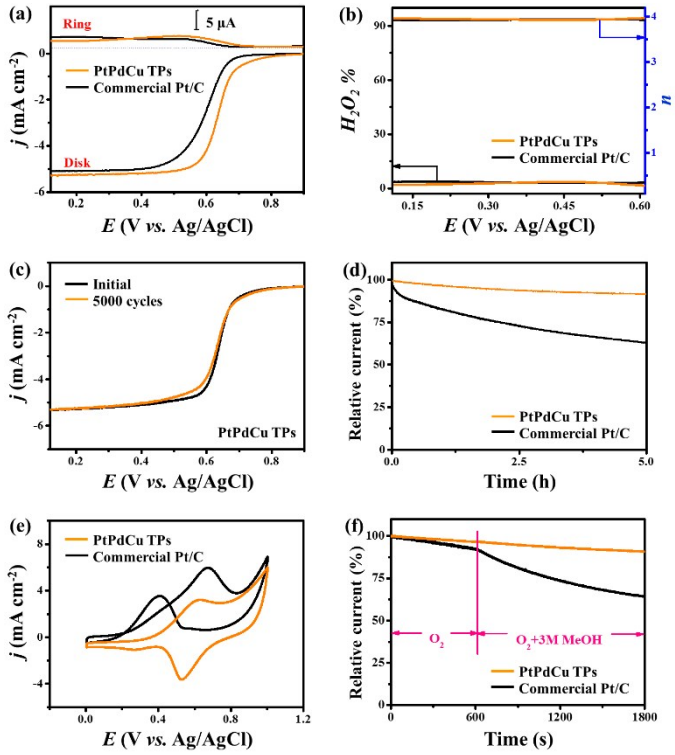

Fig. 5 (a) RRDE test of ORR. (f) H_2O_2 yield and electron transfer numbers obtained by RRDE. (c) LSVs before and after durability test and (d) *i-t* response at 0.3 V for 5 h in an O_2-saturated 0.1 M $HClO_4$ electrolyte. (e) CV curves in an O_2-saturated 0.1 M $HClO_4$ with 1 M CH_3OH. (f) *i-t* response in an O_2-saturated 0.1 M $HClO_4$ electrolyte with 3 M CH_3OH added at around 600 s.

The rotating ring disk electrode (RRDE) measurement was used to further reveal the four-electron selectivity of PtPdCu TPs. As shown in Fig. 5a, a negligible ring current (I_R) (the oxidation of H_2O_2) relative to the disc current (I_D) of the PtPdCu TPs can be observed, indicating that the evolution of H_2O_2 is greatly restrained in the ORR process. The *n* and H_2O_2 yield of PtPdCu TPs and Pt/C are calculated by using their I_R and I_D values. It is found that PtPdCu TPs show a very low H_2O_2 yield (<3.5%) and high *n* (>3.92) at the potential range of 0.6~0.1 V (Fig. 5b), which consistent with the RRDE results of Pt/C. The low H_2O_2 yield and near optimal four-electron pathway further confirm that PtPdCu TPs have a high four-electron selectivity. The stability of the PtPdCu TPs for ORR is evaluated by the accelerated durability test. After testing for 5000 cycles, the LSV curve of the PtPdCu TPs show a very minor change in E_{onset} (7 mV) and a negligible loss in limiting current density relative to the initial plot (Fig. 5c). Notably, it can be observed that the degradation for $E_{1/2}$ of the PtPdCu TPs (7 mV) is much lower compared with that of the Pt/C (28 mV), indicating an excellent stability of the PtPdCu TPs for ORR (Fig. S8). The durability of the PtPdCu TPs was further tested and compared with Pt/C by using chronoamperometric measurement at 0.3 V for 5 h. After testing for 5 h, the PtPdCu TPs lose 7.7% of its initial catalytic current density, while the decay for Pt/C is 40.2%, indicating that the PtPdCu TPs show a superior long-term durability (Fig. 5d). The methanol tolerance the PtPdCu TPs was further evaluated in an O_2-saturated $HClO_4$ with 1 M CH_3OH. The presence of a distinct ORR peak indicates that methanol has no strong effect on the ORR process of the PtPdCu TPs (Fig. 5e). Meanwhile, the ORR peak of Pt/C is completely replaced by the obvious methanol oxidation peaks, due to obstruction of the ORR process by the methanol oxidation reaction. To further confirm the high methanol-tolerance ability of the PtPdCu TPs, chronoamperometric investigations were performed. After adding 3 M methanol into the O_2-saturated electrolyte, there is no intensive current decay in the chronoamperometric response of the PtPdCu TPs, implying their high ORR selectivity and excellent methanol-tolerant ability (Fig. 5f). For comparison, there is an intensive current decay of Pt/C after injecting with 3 M CH_3OH, due to the electrochemical oxidation of CH_3OH.

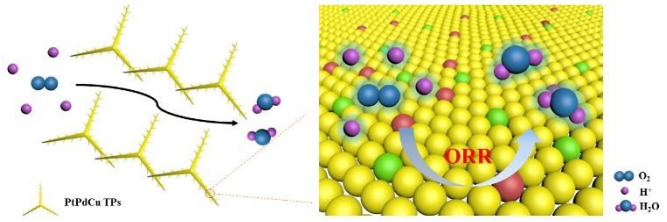

Fig. 6 Schematic illustration showing the catalytic process for ORR on the PtPdCu TPs.

The enhanced ORR performance of the PtPdCu TPs mainly originates from their hierarchically branched structure and tri-metallic composition (Fig.6). The highly branched structure provides sufficiently assessable catalytic sites, favoring a high catalytic activity for ORR. Different from spherical Pt-based nanoparticles, the branched PtPdCu TPs are unsusceptible to particle aggregation, resulting in an improved durability. With its porous self-supported structure, the PtPdCu TPs offers a higher mass transport of O_2 compared with the supported catalysts. The tri-metallic composition is also critical to the superior catalytic performance of PtPdCu TPs. The ORR performance of the PtPdCu TPs is superior to those of the PtPd and PtCu nanocrystals (NCs) which are prepared under the same synthesis condition, suggesting that the incorporation of Pd and Cu into Pt favors an enhanced ORR performance (Fig. S2b, Fig. S2c and Fig. S9). As a catalyst for ORR, alloying Pt (the metal with unsaturated *d*-orbitals) with Pd and Cu (the metals with fully occupied *d*-orbitals) can decrease the Gibbs free energy because of the coupling effect among their *d*-orbitals, resulting in an enhanced kinetics for ORR. Furthermore, owing

to the alloyed composition effect, the dissociation of adsorbed O_2 on the PtPdCu TPs also can be observably facilitated, thus leading to the reduced polarization of the dissociated O atoms' electroreduction.

Conclusions

Hierarchically branched PtPdCu TPs have been fabricated with a high yield through a one-step synthetic method in an aqueous solution. Different from previous multi-step synthesis in organic solvents, the proposed method offers a simple way to PtPdCu TPs. The PtPdCu TPs are very unique in their branched exteriors, which are quite different from previously reported tripods with smooth surfaces. The PtPdCu TPs show superior catalytic performance for ORR, which can be attributed to their spatially and locally separated branches and tri-metallic compositions. The developed fabrication method is very promising for future preparation of mutil-metallic tripods with controllable compositions and desired functions beyond electrocatalysis.

Acknowledgements

This work was financially supported by the National Natural Science Foundation of China (No. 21601154, 21776255, 21701141), and Natural Science Foundation of Zhejiang Province (No. LQ18B010005). This work was supported by the Deanship of Scientific Research (DSR), King Abdulaziz University, Jeddah, under grant No. KEP-1-130-39.

References

1 E. Ye, M. D. Regulacio, S.-Y. Zhang, X. J. Loh and M.-Y. Han, *Chem. Soc. Rev.,* 2015, **44**, 6001–6017.
2 B. Lim, M. Jiang, J. Tao, P. H. C. Camargo, Y. Zhu and Y. Xia, *Adv. Funct. Mater.,* 2009, **19**, 189–200.
3 R. Long, S. Zhou, B. J. Wiley and Y. Xiong, *Chem. Soc. Rev.,* 2014, **43**, 6288–6310.
4 Y. Xia, X. Xia and H.-C. Peng, *J. Am. Chem. Soc.,* 2015, **137**, 7947–7966.
5 N. Tian, Z.-Y. Zhou, S.-G. Sun, Y. Ding and Z. L. Wang, *Science,* 2007, **316**, 732–735.
6 J. Ding, L. Bu, S. Guo, Z. Zhao, E. Zhu, Y. Huang and X. Huang, *Nano Lett.,* 2016, **16**, 2762–2767.
7 X. Huang, Z. Zhao, Y. Chen, E. Zhu, M. Li, X. Duan and Y. Huang, *Energy Environ. Sci.,* 2014, **7**, 2957–2962.
8 L. Zhang, Q. Chen, X. Wang and Z. Jiang, *Nanoscale,* 2016, **8**, 2819–2825.
9 L. Zhang, S.-I. Choi, J. Tao, H.-C. Peng, S. Xie, Y. Zhu, Z. Xie and Y. Xia, *Adv. Funct. Mater.,* 2014, **24**, 7520–7529.
10 B. Y. Xia, H. B. Wu, N. Li, Y. Yan, X. W. Lou and X. Wang, *Angew. Chem. Int. Ed.,* 2015, **54**, 3797–3801.
11 Z. Niu, D. Wang, R. Yu, Q. Peng and Y. Li, *Chem. Sci.,* 2012, ***3***, 1925–1929.
12 S. Sun, G. Zhang, D. Geng, Y. Chen, R. Li, M. Cai and X. Sun, *Angew. Chem. Int. Ed.,* 2011, **50**, 422–426.
13 J. F. Callejas, C. G. Read, C. W. Roske, N. S. Lewis and R. E. Schaak, *Chem. Mater.,* 2016, **28**, 6017–6044.
14 H. Wang, S. Yin, Y. Li, H. Yu, C. Li, K. Deng, Y. Xu, X. Li, H. Xue and L. Wang, *J. Mater. Chem. A,* 2018, **6**, 3642–3648.
15 S. Bai, C. Wang, M. Deng, M. Gong, Y. Bai, J. Jiang and Y. Xiong, *Angew. Chem. Int. Ed.,* 2014, **53**, 12120–12124.
16 N. Du, C. Wang, X. Wang, Y. Lin, J. Jiang and Y. Xiong, *Adv. Mater., 2016*, **28**, 2077–2084.
17 S. Wang, G. Yang and S. Yang, *J. Phys. Chem. C*, 2015, **119**, 27938–27945.
18 H. Yin, S. Zhao, K. Zhao, A. Muqsit, H. Tang, L. Chang, H. Zhao, Y. Gao and Z. Tang, *Nat. Commun.,* 2015, **6**, 6430-6437.
19 B. Lim and Y. Xia, *Angew. Chem. Int. Ed.,* 2011, **50**, 76-85.
20 X. Yu, D. Wang, Q. Peng and Y. Li, *Chem. Eur. J.,* 2013, **19**, 233-239.
21 H.-S. Chen, Y.-T. Liang, T.-Y. Chen, Y.-C. Tseng, C.-W. Liu, S.-R. Chung, C.-T. Hsieh, C.-E. Lee and K.-W. Wang, *Chem. Commun.,* 2014, **50**, 11165-11168.
22 M. Rauber, I. Alber, S. Müller, R. Neumann, O. Picht, C. Roth, A. Schökel, M. E. Toimil-Molares and W. Ensinger, *Nano Lett.,* 2011, **11**, 2304-2310.
23 I. Imaz, J. Hernando, D. Ruiz-Molina and D. Maspoch, *Angew. Chem. Int. Ed.,* 2009, **48**, 2325-2329.
24 F. Yu, W. Zhou, R. M. Bellabarba and R. P. Tooze, *Nanoscale,* 2014, **6**, 1093-1098.
25 G.-R. Xu, J. Bai, L. Yao, Q. Xue, J.-X. Jiang, J.-H. Zeng, Y. Chen and J.-M. Lee, *ACS Catal.,* 2017, **7**, 452–458.
26 S. Lu, K. Eid, Y. Deng, J. Guo, L. Wang, H. Wang and H. Gu, *J. Mater. Chem. A,* 2017, **5**, 9107–9112.
27 J. Park, A. Oh, H. Baik, Y. S. Choi, S. J. Kwon and K. Lee, *Nanoscale*, 2014, **6**, 10551–10555.
28 L. Ma, C. Wang, M. Gong, L. Liao, R Long, J. Wang, D. Wu, W. Zhong, M. J. Kim, Y. Chen, Y. Xie, and Y. Xiong, *ACS Nano*, 2012, **6**, 9797-9806.
29 S. Maksimuk, X. Teng and H. Yang, *Phys. Chem. Chem. Phys.*, 2006, **8**, 4660–4663.
30 B. C. Camargo, B. Lassagne, R. Arenal, C. Gatel, T. Blon, G. Viau, L.-M. Lacroix and W. Escoffier. *Nanoscale*, 2017, **9**, 14635–14640.
31 S. Fu, C. Zhu, J. Song, M. Engelhard, H. Xia, D. Du and Y. Lin, *ACS Appl. Mater. Interfaces,* 2016, **8**, 22196–22200.
32 V. M. Dhavale and S. Kurungot, *ACS Catal.,* 2015, **5**, 1445–1452.
33 B. Jiang, C. Li, V. Malgras and Y. Yamauchi. *J. Mater. Chem. A*, 2015, **3**, 18053–18058.
34 S. Fu, C. Zhu, J. Song, P. Zhang, M. H. Engelhard, H. Xia, D. Du and Y. Lin, *Nanoscale,* 2017, **9**, 1279–1284.
35 W. Xu, S. Zhu, Y. Liang, Z. Cui, X. Yang, A. Inoue and H. Wang, *J. Mater. Chem. A,* 2017, **5**, 18793–18800.
36 S.-H. Han, J. Bai, H.-M. Liu, J.-H. Zeng, J.-X. Jiang, Y. Chen and J.-M. Lee, *ACS Appl. Mater. Interfaces,* 2016, **8**, 30948–30955.
37 Y. Shu, X. Shi, Y. Ji, Y. Wen, X. Guo, Y. Ying, Y. Wu, and H. Yang, *ACS Appl. Mater. Interfaces*, 2018, **10**, 4743–4749.
38 B. Jiang, C. Li, V. Malgras, Y. Bando and Y. Yamauchi, *Chem. Commun.,* 2016, **52**, 1186–1189.
39 B. Jiang, C. Li, M. Imura, J. Tang and Y. Yamauchi, *Adv. Sci.,*2015, **2**, 1500112.
40 L. Wang, Y. Nemoto and Y. Yamauchi, *J. Am. Chem. Soc.,* 2011, **133**, 9674–9677.
41 S. Chen, W. Sheng, N. Yabuuchi, P. J. Ferreira, L. F. Allard and Y. Shao-Horn, *J. Phys. Chem. C* 2009, **113**, 1109–1125.

View Article Online
DOI: 10.1039/C8TA01698D

Graphical Abstract

A one-step method is developed for fabrication of PtPdCu tripods with branched exteriors for oxygen reduction reaction.